Co-segregation at the surface of Pb-Bi-Ni alloys: combined *ab initio* and Monte Carlo study

1998 J. Phys.: Condens. Matter 10 5717

(http://iopscience.iop.org/0953-8984/10/26/002)

J. Phys.: Condens. Matter **10** (1998) 5717–5738. Printed in the UK PII: S0953-8984(98)92357-8

Co-segregation at the surface of Pb–Bi–Ni alloys: combined *ab initio* and Monte Carlo study

A Landa†, A Ruban‡, P Wynblatt†, H Skriver‡, A Girshick§ and V Vitek§

† Department of Materials Science and Engineering, Carnegie Mellon University, Pittsburgh, PA 15213, USA

‡ Centre for Atomic-scale Materials Physics and Physics Department, Technical University of Denmark, DK-2800 Lyngby, Denmark

§ Laboratory for Research on the Structure of Matter and Department of Materials Science and Engineering, University of Pennsylvania, Philadelphia, PA 19104, USA

Received 10 March 1998

Abstract. A recent study of a Pb–Bi–Ni alloy containing 5 at.% Bi and 0.04 at.% Ni reported a strong co-segregation of Bi and Ni at the alloy surface. We have performed *ab initio* calculations of the segregation profiles at the (111), (100) and (110) surfaces of random $Pb_{95}Bi_5$ alloys by means of the coherent potential approximation and the tight-binding linear muffin-tin-orbitals method. We have found the segregation profiles to be oscillatory (this effect is most pronounced for the (111) surface) with a strong preference for Bi to segregate to the first atom layer and depletion of Bi in the subsurface atom layer. The energetic origin of the oscillatory segregation is discussed in terms of the Connolly–Williams effective cluster interactions. In the ternary $Pb_{95}Bi_5$ + Ni alloy we have also found a tendency for Ni to segregate to the subsurface atom layer due its strong interaction with Bi, which is present at high concentrations relative to the bulk in both the first and third atom layers of the (111) surface. In order to include relaxation effects, we have performed Monte Carlo simulations, employing Finnis–Sinclair-type empirical many-body potentials, and computed the segregation profiles at the (111) surface of $Pb_{95}Bi_5$ and $Pb_{95}Bi_5$ + Ni alloys. For Pb–Bi alloys, the concentration profiles have also been found to be oscillatory, in fair agreement with results of the *ab initio* calculations. The calculations on Pb–Bi–Ni show strong segregation of Ni to the subsurface atom layer, accompanied by co-segregation of Bi to several of the outermost atom layers.

1. Introduction

The equilibrium surface composition of an alloy generally differs from its nominal bulk value. Besides its technological importance in such areas as catalysis, crystal growth, tribology, corrosion and chemosorption, this so-called *surface segregation* phenomenon also represents a serious theoretical challenge. Recent experiments, performed by Cheng and Wynblatt [1], showed that co-segregation of Bi–Ni to the surfaces of small crystals of a dilute Pb–Bi–Ni alloy changes the equilibrium crystal shape in relation to that of pure Pb, and leads to the reversible formation of {227} and {110} facets at roughening transition temperatures of 515 K and 510 K, respectively. Those authors have also reported that the above mentioned phenomenon is coupled with a compositional surface phase transition (an abrupt change in the surface concentration of Bi and Ni solute). The co-segregation phenomenon has previously been described by Cheng and Wynblatt [2] within the framework of a mean-field phenomenological model, based on nearest-neighbour (NN) interactions. However, interatomic interactions in metallic systems possess many-body character and

0953-8984/98/265717+22$19.50

are long range in origin [3], and cannot thus be properly accounted for within a pairwise NN model.

With the development of numerically efficient Green's function techniques for the self-consistent treatment of electronic structure in semi-infinite elemental metals (Skriver and Rosengaard [4]) and random alloys (Abrikosov and Skriver [5]) it has become possible to address the problem of surface segregation from first principles (see the review paper by Monnier [6] for details). In order to calculate near-surface segregation profiles and phase equilibria in alloys at finite temperature, this *ab initio* technique must be supplemented by the methods of statistical mechanics which allow the determination of the free energy and the configurational entropy. The basic feature of these methods is their phenomenological treatment of the interatomic interactions, in terms of effective potentials of Ising-like Hamiltonians, which may be obtained from first-principles total energy calculations.

In the present work, we performed first-principles calculations of the effective cluster interaction (ECI), at the low-index surfaces of a random $Pb_{95}Bi_5$ alloy, by using the structure inversion method of Connolly and Williams (CW) [7]. We then used these interactions in calculations of the surface segregation profiles within the mean-field approximation for the configurational entropy, neglecting lattice relaxation and thermal vibrations to the free energy of the alloys. We also performed calculations of ECI at the (111) surface of a $Pb_{95}Bi_5 + Ni$ alloy and investigated the possibility of formation of ordered structures at the outermost atom layers. The electronic structure and the total energy of the surfaces have been calculated by means of the linear muffin-tin-orbitals method (LMTO) in the tight-binding (TB) representation and the atomic sphere approximation (ASA), in conjunction with density functional theory in the local density approximation (DFT–LDA), the coherent potential approximation (CPA) and a Green's function technique [4, 5, 8–12]. The complete procedure is described in [13–17], where it was successfully used to calculate segregation profiles in CuNi, NiPt, PtPd and PdNi random alloys.

In order to assess relaxation and vibrational effects, we have also performed Monte Carlo (MC) simulations, employing Finnis–Sinclair-type (FS) empirical many-body potentials, and computed the segregation profiles at the (111) surface of $Pb_{95}Bi_5$ and $Pb_{95}Bi_5 + Ni$ alloys.

The paper is organized as follows. Pertinent details of the cluster expansion of the total energy of the FCC (111), (100) and (110) binary alloy, and (111) ternary alloy surfaces, the FS formalism and construction of the FS potentials for the Pb–Bi–Ni system (originally reported in [18]) are described in section 2. Details of calculations are described in section 3. Results of *ab initio* calculation of the ECI and segregation profiles for these surfaces of the $Pb_{95}Bi_5$ alloy and for the (111) surface of the $Pb_{95}Bi_5 + Ni$ alloy are given in sections 4 and 5, respectively. Results of MC simulation of surface segregation in Pb–Bi, Pb–Ni and Pb–Bi–Ni alloys are given in section 6. Our conclusions are given in section 7.

2. Theoretical background

2.1. Cluster expansion of the total energy of the FCC binary alloy surfaces

The equilibrium surface concentration profile of an alloy may be determined by the minimization of the corresponding grand potential of the surface region Ω_{surf} with respect to the alloy configuration. To describe these configurations, one can use the so-called multisite correlation functions [13, 19] $\langle \sigma_{\Lambda;i}\sigma_{\Lambda+k;j}\ldots\sigma_{\Lambda+m;l}\rangle$, where $\{\sigma_{\Lambda;p}\}$ is the Ising-spin-like variable which takes on the values $+1$ or -1, depending on the type of atom occupying site p in layer Λ. Therefore, the concentration of one of the components (Pb in the present

case) in layer Λ is then $c_\Lambda = (\sigma_\Lambda + 1)/2$, where $\sigma_\Lambda = \langle \sigma_{\Lambda;p} \rangle$ is the average spin variable in the layer. The *grand potential of the surface region* of the Ising lattice (in which the vibrational and relaxation effects are neglected) may be written as

$$\Omega_{surf}(\{\sigma_{\Lambda;i}\}, T) = E_{tot}(\{\sigma_{\Lambda;i}\}) - T S_{conf}(\{\sigma_{\Lambda;i}\}) - \mu \sum_{\Lambda=1}^{N} (\sigma_\Lambda - \sigma_b). \tag{1}$$

Here, T is the temperature, $E_{tot}(\{\sigma_{\Lambda;i}\})$ is the total energy of the surface region with a given alloy configuration $\{\sigma_{\Lambda;i}\}$, $S_{conf}(\{\sigma_{\Lambda;i}\})$ is the configurational entropy also of the surface region and μ is the effective chemical potential in the bulk. The sum in the last term runs over all N layers in the surface region, and $\sigma_b = \langle \sigma_{b;p} \rangle$ is the average spin variable in the bulk. The determination of the equilibrium concentration profile can be performed easily by mapping the free energy of the system onto a set of Ising ECIs. These ECIs may be obtained from the total energies of a pre-defined set of completely random alloys with a surface, using the structure inversion method of Connolly and Williams [7]. This method has been generalized by Ruban *et al* [13] for the (100) surface of the FCC lattice.

(i) *In the case of the FCC (100) surface*, in order to construct the corresponding Hamiltonian, one must note that there is only one kind of tetrahedron which connects the layers Λ and $\Lambda + 1$, and that this tetrahedron has two vertices in each of the layers. As illustrated in figure 1, one may therefore define six different kinds of nearest-neighbour interaction parameters which are (1) $V_\Lambda^{(1)}$, the one-site interaction in plane Λ; (2) $V_\Lambda^{(2)}$, the two-site interaction in plane Λ; (3) $V_{\Lambda+}^{(2)}$, the two-site interaction between atoms in the Λ and $\Lambda + 1$ planes; (4) $V_{\Lambda+}^{(3)}$, the three-site interaction of two atoms in plane Λ and an atom in plane $\Lambda + 1$; (5) $V_{\Lambda++}^{(3)}$, the three-site interaction of two atoms in plane $\Lambda + 1$ and an atom in plane Λ, and (6) $V_\Lambda^{(4)}$, the four-site interaction of atoms in the tetrahedron between the Λ and $\Lambda + 1$ planes. All these CW ECIs include only nearest neighbours. In order to include the interaction between the atoms in plane Λ and plane $\Lambda + 2$, one may introduce four different kinds of next-nearest-neighbour interaction parameters or so-called cluster field method interactions (CFM) (see [13, 20, 21] for details) which are (1) $u_\Lambda^{(2)}$, the two-site interaction between atoms in the Λ and $\Lambda + 2$ planes; (2) $u_{\Lambda+}^{(3)}$, the three-site interaction between two atoms in plane Λ and an atom in plane $\Lambda + 2$; (3) $u_{\Lambda++}^{(3)}$, the three-site interaction between an atom in plane Λ and two atoms in plane $\Lambda + 2$, and (4) $u_\Lambda^{(4)}$, the four-site interaction between two atoms in plane Λ and two atoms in plane $\Lambda + 2$. In the case of the FCC (100) surface, the total energy of the system can be written as

$$\begin{aligned} E_{tot}^{(100)}(\{\sigma_{\Lambda;i}\}) = E_0 + \sum_{\Lambda=1}^{N} [& V_\Lambda^{(1)} \langle \sigma_{\Lambda;i} \rangle + V_\Lambda^{(2)} \langle \sigma_{\Lambda;i} \sigma_{\Lambda;j} \rangle + V_{\Lambda+}^{(2)} \langle \sigma_{\Lambda;i} \sigma_{\Lambda+1;j} \rangle \\ & + V_{\Lambda+}^{(3)} \langle \sigma_{\Lambda;i} \sigma_{\Lambda;j} \sigma_{\Lambda+1;k} \rangle + V_{\Lambda++}^{(3)} \langle \sigma_{\Lambda;i} \sigma_{\Lambda+1;j} \sigma_{\Lambda+1;k} \rangle \\ & + V_\Lambda^{(4)} \langle \sigma_{\Lambda;i} \sigma_{\Lambda;j} \sigma_{\Lambda+1;k} \sigma_{\Lambda+1;l} \rangle + u_\Lambda^{(2)} \langle \sigma_{\Lambda;i} \sigma_{\Lambda+2;j} \rangle + u_{\Lambda+}^{(3)} \langle \sigma_{\Lambda;i} \sigma_{\Lambda;j} \sigma_{\Lambda+2;k} \rangle \\ & + u_{\Lambda++}^{(3)} \langle \sigma_{\Lambda;i} \sigma_{\Lambda+2;j} \sigma_{\Lambda+2;k} \rangle + u_\Lambda^{(4)} \langle \sigma_{\Lambda;i} \sigma_{\Lambda;j} \sigma_{\Lambda+2;k} \sigma_{\Lambda+2;l} \rangle] \end{aligned} \tag{2}$$

where E_0 is a reference energy.

(ii) *In the case of the FCC (111) surface*, as illustrated in figure 2, there are two kinds of tetrahedron which connect the layers Λ and $\Lambda + 1$: one tetrahedron has three vertices on layer Λ and one on layer $\Lambda + 1$; the other one has a vertex on layer Λ and three vertices on layer $\Lambda + 1$. One may therefore define eight different kinds of nearest-neighbour interaction parameters for this surface. In addition to $V_{\Lambda+}^{(3)}$ and $V_{\Lambda++}^{(3)}$, which have the same meaning as in the case of the FCC (100) surface, there is a term $V_\Lambda^{(3)}$, which represents the three-site

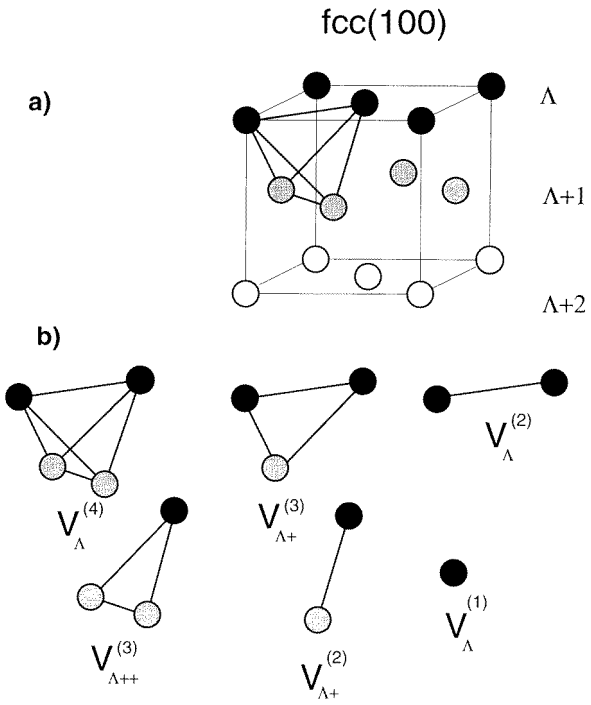

Figure 1. Sketch of included cluster interactions in the effective Hamiltonian (2). (a) The cubic FCC unit cell with Λ numbering the (100) layers. We have included up to tetrahedral nearest-neighbour contributions. (b) The inequivalent types of cluster interaction, defined on this tetrahedron. The filled, grey and open circles denote the atoms of the Λ, $\Lambda+1$ and $\Lambda+2$ planes, respectively.

interaction in plane Λ. Instead of the FCC (100) generic four-site interaction between two atoms in plane Λ and two atoms in plane $\Lambda+1$, there is a term $V_{\Lambda}^{(4)}$, representing the four-site interaction between three atoms in plane Λ and one atom in plane $\Lambda+1$, and $V_{\Lambda+}^{(4)}$, representing the four-site interaction between one atom in plane Λ and three atoms in plane $\Lambda+1$. In the case of the FCC (111) surface, the total energy of the system, with account of the next-nearest-neighbour interactions, can be written as

$$\begin{aligned}E_{tot}^{(111)}(\{\sigma_{\Lambda;i}\}) = E_0 + \sum_{\Lambda=1}^{N}[&V_{\Lambda}^{(1)}\langle\sigma_{\Lambda;i}\rangle + V_{\Lambda}^{(2)}\langle\sigma_{\Lambda;i}\sigma_{\Lambda;j}\rangle + V_{\Lambda+}^{(2)}\langle\sigma_{\Lambda;i}\sigma_{\Lambda+1;j}\rangle \\ &+V_{\Lambda+}^{(3)}\langle\sigma_{\Lambda;i}\sigma_{\Lambda;j}\sigma_{\Lambda;k}\rangle + V_{\Lambda+}^{(3)}\langle\sigma_{\Lambda;i}\sigma_{\Lambda;j}\sigma_{\Lambda+1;k}\rangle + V_{\Lambda++}^{(3)}\langle\sigma_{\Lambda;i}\sigma_{\Lambda+1;j}\sigma_{\Lambda+1;k}\rangle \\ &+V_{\Lambda}^{(4)}\langle\sigma_{\Lambda;i}\sigma_{\Lambda;j}\sigma_{\Lambda;k}\sigma_{\Lambda+1;l}\rangle + V_{\Lambda+}^{(4)}\langle\sigma_{\Lambda;i}\sigma_{\Lambda+1;j}\sigma_{\Lambda+1;k}\sigma_{\Lambda+1;l}\rangle \\ &+u_{\Lambda}^{(2)}\langle\sigma_{\Lambda;i}\sigma_{\Lambda+2;j}\rangle + u_{\Lambda+}^{(3)}\langle\sigma_{\Lambda;i}\sigma_{\Lambda;j}\sigma_{\Lambda+2;k}\rangle + u_{\Lambda++}^{(3)}\langle\sigma_{\Lambda;i}\sigma_{\Lambda+2;j}\sigma_{\Lambda+2;k}\rangle \\ &+u_{\Lambda}^{(4)}\langle\sigma_{\Lambda;i}\sigma_{\Lambda;j}\sigma_{\Lambda+2;k}\sigma_{\Lambda+2;l}\rangle].\end{aligned} \tag{3}$$

(iii) *In the case of the FCC (110) surface*, in order to construct the corresponding Hamiltonian one must note that there is only one kind of tetrahedron which connects the layers Λ, $\Lambda+1$ and $\Lambda+2$. This tetrahedron has a single vertex in each of the layers Λ and $\Lambda+2$ and two vertices in layer $\Lambda+1$. As illustrated in figure 3, one may therefore define eight different kinds of nearest-neighbour interaction parameters for this surface.

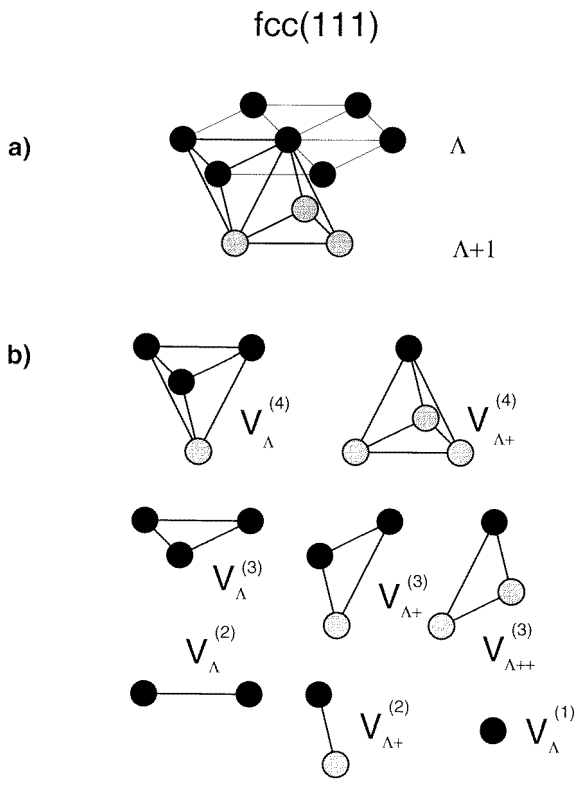

Figure 2. Sketch of included cluster interactions in the effective Hamiltonian (3). (a) The tetrahedron of the four closest neighbours belonging to the (111) plane in the FCC lattice. (b) The inequivalent types of cluster interaction, defined on this tetrahedron. Notations as in figure 1.

In addition to $V_{\Lambda}^{(2)}$ and $V_{\Lambda+}^{(2)}$, there is a term $V_{\Lambda++}^{(2)}$, representing the two-site interaction between atoms in the Λ and $\Lambda+2$ planes; and in addition to $V_{\Lambda+}^{(3)}$ and $V_{\Lambda++}^{(3)}$, there is a term $V_{\Lambda+++}^{(3)}$, representing the three-site interaction between single atoms in planes Λ, $\Lambda+1$ and $\Lambda+2$. Finally, there is a term $V_{\Lambda}^{(4)}$, representing the four-site interaction between an atom in the plane Λ, two atoms in the plane $\Lambda+1$ and an atom in the plane $\Lambda+2$. In the case of the FCC (110) surface, it is impossible to separate out the next-nearest-neighbour interaction parameters in the same manner as has been done for the other two low-index orientations. These interactions correspond to atoms belonging to the same layer Λ, or to atoms belonging to the Λ and $\Lambda+2$ layers (these interactions have already been accounted for in the CW scheme). In order to improve the convergence of the cluster expansion for the FCC (110) surface, we have also added a term $V_{\Lambda+}^{(4)}$, the four-site interaction between two atoms in the plane Λ and two atoms in the plane $\Lambda+1$. In the case of the FCC (110) surface, the total energy of the system can be written as

$$E_{tot}^{(110)}(\{\sigma_{\Lambda;i}\}) = E_0 + \sum_{\Lambda=1}^{N}[V_{\Lambda}^{(1)}\langle\sigma_{\Lambda;i}\rangle + V_{\Lambda}^{(2)}\langle\sigma_{\Lambda;i}\sigma_{\Lambda;j}\rangle + V_{\Lambda+}^{(2)}\langle\sigma_{\Lambda;i}\sigma_{\Lambda+1;j}\rangle$$
$$+V_{\Lambda++}^{(2)}\langle\sigma_{\Lambda;i}\sigma_{\Lambda+2;j}\rangle + V_{\Lambda+}^{(3)}\langle\sigma_{\Lambda;i}\sigma_{\Lambda;j}\sigma_{\Lambda+1;k}\rangle + V_{\Lambda++}^{(3)}\langle\sigma_{\Lambda;i}\sigma_{\Lambda+1;j}\sigma_{\Lambda+1;k}\rangle$$

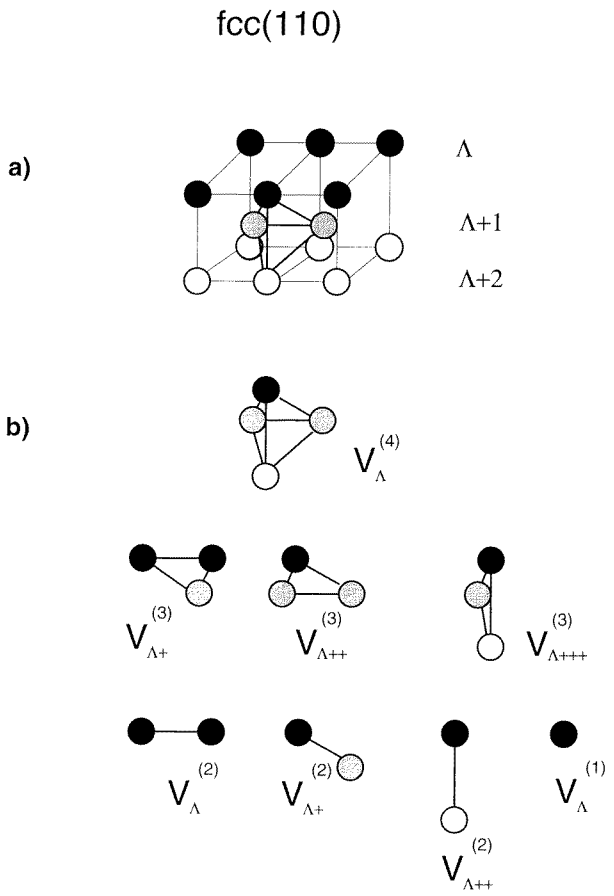

Figure 3. Sketch of included cluster interactions in the effective Hamiltonian (4). (a) The tetrahedron of the four closest neighbours belonging to the (110) plane in the FCC lattice. (b) The inequivalent types of cluster interaction, defined on this tetrahedron. Notations as in figure 1.

$$+V^{(3)}_{\Lambda+++}\langle\sigma_{\Lambda;i}\sigma_{\Lambda+1;j}\sigma_{\Lambda+2;k}\rangle + V^{(4)}_{\Lambda}\langle\sigma_{\Lambda;i}\sigma_{\Lambda+1;j}\sigma_{\Lambda+1;k}\sigma_{\Lambda+2;l}\rangle$$
$$+V^{(4)}_{\Lambda+}\langle\sigma_{\Lambda;i}\sigma_{\Lambda;j}\sigma_{\Lambda+1;k}\sigma_{\Lambda+1;l}\rangle]. \tag{4}$$

In a layer-wise, completely random alloy where $\langle\sigma_{\Lambda;i}\sigma_{\Lambda';j}\ldots\sigma_{\Lambda'';k}\rangle = \sigma_{\Lambda}\sigma_{\Lambda'}\ldots\sigma_{\Lambda''}$, the total energy (2)–(4) simplifies to the forms

$$E^{(100)}_{tot\,(rand)}(\{\sigma_\Lambda\}) = E_0 + \sum_{\Lambda=1}^{N}[V^{(1)}_{\Lambda}\sigma_{\Lambda} + V^{(2)}_{\Lambda}\sigma^2_{\Lambda} + V^{(2)}_{\Lambda+}\sigma_{\Lambda}\sigma_{\Lambda+1} + V^{(3)}_{\Lambda+}\sigma^2_{\Lambda}\sigma_{\Lambda+1}$$
$$+V^{(3)}_{\Lambda++}\sigma_{\Lambda}\sigma^2_{\Lambda+1} + V^{(4)}_{\Lambda}\sigma^2_{\Lambda}\sigma^2_{\Lambda+1} + u^{(2)}_{\Lambda}\sigma_{\Lambda}\sigma_{\Lambda+2} + u^{(3)}_{\Lambda+}\sigma^2_{\Lambda}\sigma_{\Lambda+2} + u^{(3)}_{\Lambda++}\sigma_{\Lambda}\sigma^2_{\Lambda+2}$$
$$+u^{(4)}_{\Lambda}\sigma^2_{\Lambda}\sigma^2_{\Lambda+2}] \tag{5}$$
$$E^{(111)}_{tot\,(rand)}(\{\sigma_\Lambda\}) = E_0 + \sum_{\Lambda=1}^{N}[V^{(1)}_{\Lambda}\sigma_{\Lambda} + V^{(2)}_{\Lambda}\sigma^2_{\Lambda} + V^{(2)}_{\Lambda+}\sigma_{\Lambda}\sigma_{\Lambda+1} + V^{(3)}_{\Lambda}\sigma^3_{\Lambda} + V^{(3)}_{\Lambda+}\sigma^2_{\Lambda}\sigma_{\Lambda+1}$$
$$+V^{(3)}_{\Lambda++}\sigma_{\Lambda}\sigma^2_{\Lambda+1} + V^{(4)}_{\Lambda}\sigma^3_{\Lambda}\sigma_{\Lambda+1} + V^{(4)}_{\Lambda+}\sigma_{\Lambda}\sigma^3_{\Lambda+1} + u^{(2)}_{\Lambda}\sigma_{\Lambda}\sigma_{\Lambda+2} + u^{(3)}_{\Lambda+}\sigma^2_{\Lambda}\sigma_{\Lambda+2}$$

$$+u^{(3)}_{\Lambda++}\sigma_\Lambda\sigma^2_{\Lambda+2}+u^{(4)}_\Lambda\sigma^2_\Lambda\sigma^2_{\Lambda+2}] \tag{6}$$

$$E^{(110)}_{tot\,(rand)}(\{\sigma_\Lambda\})=E_0+\sum_{\Lambda=1}^{N}[V^{(1)}_\Lambda\sigma_\Lambda+V^{(2)}_\Lambda\sigma^2_\Lambda+V^{(2)}_{\Lambda+}\sigma_\Lambda\sigma_{\Lambda+1}+V^{(2)}_{\Lambda++}\sigma_\Lambda\sigma_{\Lambda+2}$$
$$+V^{(3)}_{\Lambda+}\sigma^2_\Lambda\sigma_{\Lambda+1}+V^{(3)}_{\Lambda++}\sigma_\Lambda\sigma^2_{\Lambda+1}+V^{(3)}_{\Lambda+++}\sigma_\Lambda\sigma_{\Lambda+1}\sigma_{\Lambda+2}+V^{(4)}_\Lambda\sigma_\Lambda\sigma^2_{\Lambda+1}\sigma_{\Lambda+2}$$
$$+V^{(4)}_{\Lambda+}\sigma^2_\Lambda\sigma^2_{\Lambda+1}]. \tag{7}$$

For close-packed surfaces, it usually suffices to consider the ECIs to be different from their respective bulk values in the four outermost layers, thus the concentrations in the fifth and deeper layers were fixed at a composition $Pb_{95}Bi_5$, providing a smooth fit to the bulk region. In total, we treated 39 configurations for the (111) face, 29 for the (100) face, and 27 for the (110) face (see the appendix, tables A1–A3). On the basis of these calculations, we extracted CWM and CFM interactions by inversion of (5), (6) and (7) for the (100), (111) and (110) surfaces, respectively.

Finally, we calculated the equilibrium concentration profiles within the single-site mean-field (MF) approximation for the configurational entropy. As shown in [5, 13], short-range order has little effect on the equilibrium composition of an alloy surface at temperatures above the bulk order–disorder temperature. Thus, neglecting lattice relaxation and thermal vibrations:

$$S_{conf}=-k_B\sum_{\Lambda=1}^{N}[c_\Lambda\ln c_\Lambda+(1-c_\Lambda)\ln(1-c_\Lambda)]. \tag{8}$$

2.2. Cluster expansion of the total energy of the FCC (111) ternary alloy surface

There are two different ways to deal with multicomponent systems. One can still use the 'Ising-like' model with only one spin variable $\sigma_{\Lambda;i}$ [22] or what is much more natural, to make a cluster expansion in the $n-1$ dimensional space of spin variables, where n is the number of the components in the system. In this case the spin variables have an additional index, say p, corresponding to the alloy species: $\sigma_{\Lambda;pi}$. Hence, in the case of a ternary system A–B–C we will have two independent spin variables for each lattice site $\sigma_{\Lambda;Bi}$ and $\sigma_{\Lambda;Ci}$.

The general expression for the cluster expansion of the total energy can be written in a way similar to that for the two-component systems:

$$E_{tot}(\{\sigma_{\Lambda;pi}\})=E_0+\sum_{\Lambda=1}^{N}\Bigg\{\sum_{p=B,C}V^{(1)}_{\Lambda;p}\langle\sigma_{\Lambda;pi}\rangle$$
$$+\sum_{p,p'=B,C}[V^{(2)}_{\Lambda;pp'}\langle\sigma_{\Lambda;pi}\sigma_{\Lambda;p'j}\rangle+V^{(2)}_{\Lambda+;pp'}\langle\sigma_{\Lambda;pi}\sigma_{\Lambda+1;p'j}\rangle+\cdots]$$
$$+\sum_{p,p',p''=B,C}[V^{(3)}_{\Lambda;pp'p''}\langle\sigma_{\Lambda;pi}\sigma_{\Lambda;p'j}\sigma_{\Lambda;p''k}\rangle$$
$$+V^{(3)}_{\Lambda+;pp'p''}\langle\sigma_{\Lambda;pi}\sigma_{\Lambda+1;p'j}\sigma_{\Lambda+1;p''k}\rangle+\cdots]\Bigg\}. \tag{9}$$

As the first approximation, for the case of a ternary system, we use a restricted form of this expansion without multisite interactions:

$$E_{tot}(\{\sigma_{\Lambda;pi}\})=E_0+\sum_{\Lambda=1}^{N}\{V^{(1)}_{\Lambda;B}\langle\sigma_{\Lambda;Bi}\rangle+V^{(1)}_{\Lambda;C}\langle\sigma_{\Lambda;Ci}\rangle+V^{(2)}_{\Lambda;BB}\langle\sigma_{\Lambda;Bi}\sigma_{\Lambda;Bj}\rangle$$
$$+V^{(2)}_{\Lambda;CC}\langle\sigma_{\Lambda;Ci}\sigma_{\Lambda;Cj}\rangle+V^{(2)}_{\Lambda;BC}\langle\sigma_{\Lambda;Bi}\sigma_{\Lambda;Cj}\rangle+V^{(2)}_{\Lambda+;BB}\langle\sigma_{\Lambda;Bi}\sigma_{\Lambda+1;Bj}\rangle$$

$$+V^{(2)}_{\Lambda+;CC}\langle\sigma_{\Lambda;C_i}\sigma_{\Lambda+1;Cj}\rangle + V^{(2)}_{\Lambda+;BC}(\langle\sigma_{\Lambda;Bi}\sigma_{\Lambda+1;Cj}\rangle$$
$$+\langle\sigma_{\Lambda;Ci}\sigma_{\Lambda+1;Bj}\rangle) + V^{(2)}_{\Lambda++;BB}\langle\sigma_{\Lambda;Bi}\sigma_{\Lambda+2;Bj}\rangle + V^{(2)}_{\Lambda++;CC}\langle\sigma_{\Lambda;Ci}\sigma_{\Lambda+2;Cj}\rangle$$
$$+V^{(2)}_{\Lambda++;BC}(\langle\sigma_{\Lambda;Bi}\sigma_{\Lambda+2;Cj}\rangle + \langle\sigma_{\Lambda;Ci}\sigma_{\Lambda+2;Bj}\rangle)\}. \tag{10}$$

In this case, as the interaction parameters are concentration independent quantities, one may establish an explicit connection between interactions in the ternary system and the corresponding binaries:

$$V^{(1)}_{\Lambda;B} = V^{(1)\,AB}_{\Lambda} + 2W_{\Lambda} + W_{(\Lambda-2)++} + W_{(\Lambda-1)+} + W_{(\Lambda)+}$$
$$V^{(1)}_{\Lambda;C} = V^{(1)\,AC}_{\Lambda} + 2W_{\Lambda} + W_{(\Lambda-2)++} + W_{(\Lambda-1)+} + W_{(\Lambda)+}$$
$$V^{(2)}_{\Lambda;BB} = V^{(1)\,AB}_{\Lambda} \qquad V^{(2)}_{\Lambda+;BB} = V^{(2)\,AB}_{\Lambda+} \qquad V^{(2)}_{\Lambda++;BB} = V^{(2)\,AB}_{\Lambda++}$$
$$V^{(2)}_{\Lambda;CC} = V^{(2)\,AC}_{\Lambda} \qquad V^{(2)}_{\Lambda+;CC} = V^{(2)\,AC}_{\Lambda+} \qquad V^{(2)}_{\Lambda++;CC} = V^{(2)\,AC}_{\Lambda++}$$
$$V^{(2)}_{\Lambda;BC} = 2W_{\Lambda} \qquad V^{(2)}_{\Lambda+;BC} = W_{\Lambda+} \qquad V^{(2)}_{\Lambda++;BC} = W_{\Lambda++} \tag{11}$$

where $V^{(n)PQ}$ are the n-site interactions of the P–Q binary system, and

$$W_{\Lambda} = \tfrac{1}{2}[V^{(2)\,AB}_{\Lambda} + V^{(2)\,AC}_{\Lambda} - V^{(2)\,BC}_{\Lambda}]$$
$$W_{\Lambda+} = \tfrac{1}{2}[V^{(2)\,AB}_{\Lambda+} + V^{(2)\,AC}_{\Lambda+} - V^{(2)\,BC}_{\Lambda+}]$$
$$W_{\Lambda++} = \tfrac{1}{2}[V^{(2)\,AB}_{\Lambda++} + V^{(2)\,AC}_{\Lambda++} - V^{(2)\,BC}_{\Lambda++}]. \tag{12}$$

2.3. Many-body potential formalism: construction of the FS potentials for the Pb–Bi–Ni system

An MC computational approach for the study of surface segregation in metallic systems (e.g. Ni–Cu) was developed by Foiles [23] and subsequently used to study Cu–Au and Cu–Ag surfaces [24, 25]. In that approach, many-body interatomic interactions were described by means of the embedded atom method (EAM) [26]. EAM potentials are not currently available for Pb-based alloys.

Pure Pb has been successfully studied by means of a so-called 'glue' potential developed by Ercolessi *et al* [27, 28]. However, this potential is difficult to apply to the case of binary alloys. One attractive option for constructing suitable interatomic potentials for the Pb–Bi–Ni system is the Finnis–Sinclair (FS) scheme [29, 30]. FS potentials are a special case of the embedded atom approximation, in which the embedding function is the square root of the density. This scheme allows a simple incorporation of inter-species interactions which involves fitting the experimental energies of mixing [31, 32]. The construction of such potentials for the Pb–Bi–Ni system has been recently reported in [18]. Here, we only briefly summarize the main criteria used in fitting procedure.

The potentials describing Ni–Ni and Bi–Bi interactions were taken to be the same as those previously fitted to the equilibrium properties of pure Ni and Bi [32, 33]: the lattice parameter, the cohesive energy, elastic moduli and the lower bound of the unrelaxed vacancy formation energy. The above approach was used in [18] to construct potentials describing Pb–Pb interactions. For the Pb–Bi system, the FS potential has been fitted so as to reproduce the experimental enthalpy of mixing for the disordered solid solution and the equilibrium lattice constants (a and c/a) for the ordered Pb_3Bi HCP phase. For Pb–Ni and Bi–Ni systems, the FS potential has been fitted to several quantities, calculated for hypothetical Pb_3Ni ($L1_2$) and BiNi (B_2) compounds within a full-potential linear-muffin-tin orbitals (FP–LMTO) method in the LDA approximation [34].

3. Computational details

We have employed two different computational techniques to obtain segregation profiles for low-index surfaces of the Pb–Bi–Ni alloy. Here we briefly summarize the computational approaches.

3.1. LMTO–CPA calculations

To obtain the multisite (CWM and CFM) interactions we have performed total energy calculations for a series of random (100), (111) and (110) surfaces of the $Pb_{95}Bi_5$ alloy by means of the TB–LMTO–CPA–ASA and Green's function technique. The surface regions were treated self-consistently and consisted of nine or 12 layers of atomic spheres and three or four layers of vacuum spheres for (111), (100) or (110) planes, respectively. The screened impurity model was used for the electrostatic one-electron potential and the energy of the charged impurity in the electroneutral effective medium, with a parameter: $\beta = 0.6$ [35]. All calculations were performed spin restricted [5, 8]. The valence electrons were included in the self-consistent calculations with $l_{max} = 2$ and the core electrons were recalculated at each LDA iteration. For exchange and correlation, we used the Perdew–Zunger parametrization [36] of the many-body calculations of Ceperley and Alder [37]. The individual atomic sphere radii were set equal to the average atomic Wigner–Seitz radius (3.6557 au) of the bulk $Pb_{95}Bi_5$ alloy (the equilibrium lattice parameter of this alloy obtained in the bulk calculations is 4.948 Å, in good agreement with the experimental value of 4.943 Å [38]). Integration over the Brillouin zone was performed by the special point technique [39] with 505 $\boldsymbol{k}$ points in the irreducible wedge (1/48) of the FCC Brillouin zone in the bulk calculations. For similar surface calculations, 36, 90 and 64 special $\boldsymbol{k}$ points in the irreducible polygon (1/8, 1/3 and 1/4) of the 2D Brillouin zone were used for FCC (100), (111) and (110) surfaces, respectively. The moments of the state density needed for the kinetic energy and for the valence charge density were calculated by integrating the Green's function on a complex energy contour using a Gaussian integration technique with 16 points on a semicircle (with diameter equal to 1.3 Ryd) enclosing the occupied states. The convergence criteria for the total energy was 0.001 mRyd. The equilibrium lattice parameter and corresponding ground state energy of a given alloy were obtained on the basis of five self-consistent calculations of the total energy close to the equilibrium lattice parameter and a subsequent fit to a Morse-type equation of state [40].

3.2. MC simulations

As mentioned above, the approach used here is that of Foiles [23], where the system under consideration is allowed to evolve towards equilibrium by means of three types of change: (a) small displacements in the positions of atoms, which simulate atomic vibration and relaxation; (b) spatial expansion and contraction of the entire system, to simulate thermal expansion effects, and (c) arbitrary changes in chemical type, so as to allow the system to reach compositional equilibrium.

The computational cell for simulations of the (111) surface (a so-called 'surface' cell) consisted of a rectangular prism with [111], $[1\bar{1}0]$ and $[11\bar{2}]$ directions lying parallel to the z, x and y coordinate axes, respectively. In the thickness direction, the slab consisted of 22 (111) layers, each containing 200 atoms, resulting in 4400 atoms in the 'surface' computational cell. Periodic boundary conditions were applied in the x and y directions. The equilibrium lattice constant was obtained from so-called 'bulklike' simulations. The

'bulklike' computational cell was selected to have a cubic shape composed of 500 atoms, and bounded by {100} faces, with 3D periodic boundary conditions. A prescribed value of the chemical potential difference ($\Delta\mu$) was used to fix the equilibrium chemical composition of the system at a given temperature. This difference is generally not known and must be determined by performing series of preliminary (trial and error) MC simulations with different values of $\Delta\mu$ on a 'bulklike' computational cell in order to obtain any desired composition. For example in order to fix the equilibrium chemical composition of $Pb_{95}Bi_5$ at $T = 500$ K, it was necessary to use a value of the chemical potential difference $\Delta\mu_1 = \mu_{Bi} - \mu_{Pb} = 0.156$ eV, and for Pb–0.040 at.% Ni a chemical potential difference of $\Delta\mu_2 = \mu_{Ni} - \mu_{Pb} = -2.3717$ eV was found. For the ternary Pb–5 at.% Bi–0.04 at.% Ni alloy (with the same concentrations of Bi and Ni) at the same temperature, these values were found to be $\Delta\mu_1 = 0.156$ eV and $\Delta\mu_2 = -2.550$ eV.

4. Results of *ab initio* calculation of the segregation profiles for low-index surfaces of the $Pb_{95}Bi_5$ alloy

Before performing time-consuming calculations of the segregation profiles for $Pb_{95}Bi_5$ alloy, we calculated the surface energies for Pb low-index planes in order to test the *ab initio* approach selected. As a result we obtained: $\gamma_{111} = 36.21$ meV Å^{-2}, $\gamma_{100} = 38.56$ meV Å^{-2} and $\gamma_{110} = 39.18$ meV Å^{-2}, i.e. ratios $\gamma_{100}/\gamma_{111} = 1.06$, and $\gamma_{110}/\gamma_{111} = 1.08$. These theoretical results are in a fair agreement with experimental observation by Heyraud and Metois [41]: at $T = 573$ K, $\gamma_{100}/\gamma_{111} = 1.021$ and $\gamma_{110}/\gamma_{111} = 1.062$. For comparison, we note that the empirical many-body 'glue' potential [28], fitted to the surface energy of the Pb(100) plane ($\gamma_{100} = 38.00$ meV Å^{-2}) and successfully used to study roughening and premelting of the Pb(110) surface [42, 43], 'gives' a much higher relative value for the Pb(110) surface energy ($\gamma_{110}/\gamma_{111} = 1.115$).

4.1. $Pb_{95}Bi_5$(111) alloy surface

The nearest (CW) and next-nearest (CF) ECIs for the $Pb_{95}Bi_5$(111) alloy surface calculated on the basis of the LMTO–CPA total energies are presented in table 1. Figure 4 shows the calculated equilibrium segregation profiles for the (111) surface of a random $Pb_{95}Bi_5$ alloy at several different temperatures [44]. We obtain oscillatory segregation profiles, with a strong segregation of Bi to the first surface layer, and a depletion of Bi in the second layer. As has been shown in [14, 16, 17], the 'point' ECI, $V_\Lambda^{(1)} - V_{bulk}^{(1)}$, represents a linear contribution to the segregation energy and thus its sign and value mainly control the segregation to a given layer. For example, a positive (negative) value of this term indicates that a negative (positive) σ_Λ would reduce the total energy of the system and hence c_Λ is expected to be less (more) than 0.95. Therefore, the oscillatory behaviour of the subsurface concentration is a direct consequence of the different signs of the one-site interactions of Bi on the first and the second layers. $V_\Lambda^{(2)}$ and $V_{\Lambda+}^{(2)}$ interactions play a similar role, but since they are multiplied by the product of two spin variables in (6), they typically influence the absolute value of the segregation but not its sign. In the case of the $Pb_{95}Bi_5$(111) alloy surface, both intralayer ($V_\Lambda^{(2)}$) and interlayer ($V_{\Lambda+}^{(2)}$) interactions are positive which reflects a slight ordering tendency known to exist in the bulk Pb–Bi alloy [38] (where Pb_3Bi is an ordered HCP (A_3) phase). The most important term (after $V_\Lambda^{(1)} - V_{bulk}^{(1)}$) in the formation of the segregation profile is $V_{\Lambda+}^{(2)}$. This governs the composition in the Λth layer relative to that of the neighbouring $(\Lambda + 1)$th layer, and positive values for these interactions will favour a

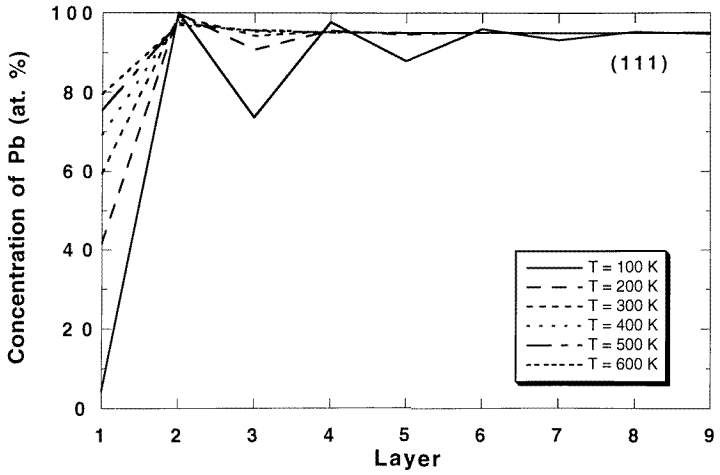

Figure 4. *Ab initio* calculated equilibrium segregation profiles at the (111) surface of the disordered $Pb_{95}Bi_5$ alloy at the indicated temperatures.

segregation profile where the layers Λ and $\Lambda+1$ are enriched by atoms of the opposite type. For the $Pb_{95}Bi_5(111)$ alloy surface, $V^{(2)}_{\Lambda+} > V^{(2)}_{\Lambda}$, which means that the tendency for interlayer ordering is stronger than that for intralayer ordering. (The opposite trend $V^{(2)}_{\Lambda+} < V^{(2)}_{\Lambda}$ has been found for the $Pt_{50}Ni_{50}(111)$ alloy surface [14] where the compositional oscillation has been found to be weak.)

Table 1. The CW and CF effective cluster interactions for the $Pb_{95}Bi_5(111)$ surface in K.

	CW							
Λ	$V^{(1)}_{\Lambda} - V^{(1)}_{bulk}$	$V^{(2)}_{\Lambda}$	$V^{(2)}_{\Lambda+}$	$V^{(3)}_{\Lambda}$	$V^{(3)}_{\Lambda+}$	$V^{(3)}_{\Lambda++}$	$V^{(4)}_{\Lambda}$	$V^{(4)}_{\Lambda+}$
1	499.38	231.54	370.45	−109.27	−134.61	107.51	136.07	−95.50
2	−505.32	190.13	203.77	42.30	47.12	47.14	−44.31	−14.54
3	−327.27	192.33	307.65	−19.88	37.42	82.17	−23.19	−72.03
4	0.00	191.36	191.36	15.75	47.24	47.24	−72.03	−72.03

	CF			
Λ	$u^{(2)}_{\Lambda}$	$u^{(3)}_{\Lambda+}$	$u^{(3)}_{\Lambda++}$	$V^{(4)}_{\Lambda}$
1	−135.05	−5.28	−13.95	10.98
2	−35.69	−15.39	−12.91	0.03
3	−35.69	−15.39	−12.91	0.03
4	−35.69	−15.39	−12.91	0.03

4.2. $Pb_{95}Bi_5(100)$ alloy surface

The nearest and next-nearest ECIs for the $Pb_{95}Bi_5(100)$ alloy surface are presented in table 2. Figure 5 shows the calculated equilibrium segregation profiles for the (100) surface of a random $Pb_{95}Bi_5$ alloy at several different temperatures. As in the case of the (111) surface,

we find a strong segregation of Bi to the first surface layer and a depletion of Bi in the second layer, which remains almost unchanged as the temperature increases. (This behaviour can again be explained in terms of the point interaction $V_{\Lambda}^{(1)} - V_{bulk}^{(1)}$: it has a high positive value on the first layer and a high negative value on the second one.) However for this surface, we observed a monotonic decrease of Pb concentration from ∼1 toward the bulk value of 0.95 between the second and the fourth layers. This could be explained by the fact that the point interaction $V_{3}^{(1)} - V_{bulk}^{(1)}$ is an order of magnitude smaller than the point interaction on the first and the second layers. Also, $V_{2+}^{(2)} < V_{2}^{(2)}$, which indicates preference of intralayer ordering over interlayer ordering in the second layer (the oscillations of the segregation profiles are suppressed).

Table 2. The CW and CF effective cluster interactions for the $Pb_{95}Bi_5(100)$ surface in K.

	CW						CF			
Λ	$V_{\Lambda}^{(1)} - V_{bulk}^{(1)}$	$V_{\Lambda}^{(2)}$	$V_{\Lambda+}^{(2)}$	$V_{\Lambda+}^{(3)}$	$V_{\Lambda++}^{(3)}$	$V_{\Lambda}^{(4)}$	$u_{\Lambda}^{(2)}$	$u_{\Lambda+}^{(3)}$	$u_{\Lambda++}^{(3)}$	$V_{\Lambda}^{(4)}$
1	825.18	72.68	344.78	20.42	50.07	63.15	−175.17	1.89	−1.28	−45.02
2	−579.18	157.34	143.75	−26.61	5.88	−56.87	−17.08	−15.26	−6.10	−3.96
3	−38.66	221.01	324.89	14.52	−34.61	−36.03	−17.08	−15.26	−6.10	−3.96
4	0.00	184.10	368.20	−10.04	−10.04	−36.03	−17.08	−15.26	−6.10	−3.96

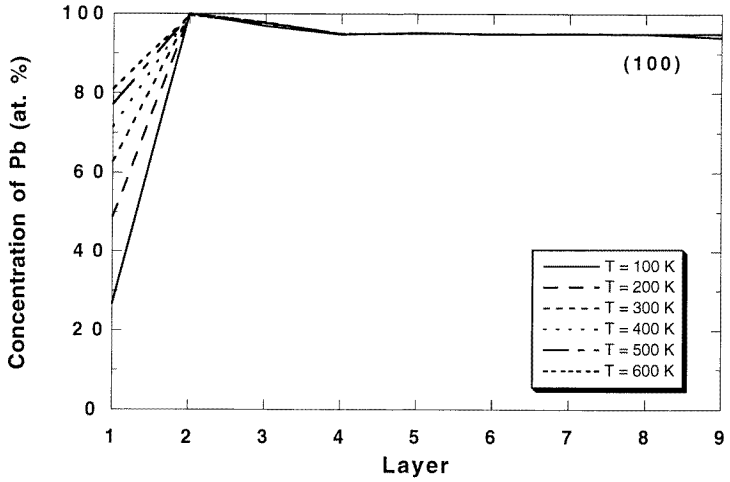

Figure 5. *Ab initio* calculated equilibrium segregation profiles at the (100) surface of the disordered $Pb_{95}Bi_5$ alloy at the indicated temperatures.

4.3. $Pb_{95}Bi_5$(110) alloy surface

We have calculated the segregation energy of Bi in the first three outermost layers of the $Pb_{95}Bi_5(110)$ alloy surface according to the definition [15, 17, 45]:

$$E_{\Lambda}^{segr,Bi} = -E_{\Lambda}^{segr,Pb} = -\frac{\partial E_{surf}}{\partial c_{\Lambda}} \tag{13}$$

where the derivative is taken at a given fixed concentration profile. The calculated values of the segregation energies are −0.221 eV/atom, −0.080 eV/atom and −0.005 eV/atom for the first, second and third atom layers of the $Pb_{95}Bi_5$(110) alloy surface, respectively. They are all negative and decrease rapidly in absolute value as the layer number increases (the bulk region is reached for $\Lambda = 3$). In the absence of contributions other than point interactions, Bi should strongly segregate on the surface $Pb_{95}Bi_5$(110) layer and its concentration should gradually decrease to the bulk value of 5% by the third layer. However as we can see, other ECIs play an important role in the formation of the segregation profiles.

In table 3 we show the CW ECIs calculated for the $Pb_{95}Bi_5$(110) alloy surface (also $V^{(4)}_{\Lambda+} = 16.14$ K, 28.79 K, −16.07 K and −16.07 K on the first, second, third and fourth planes, respectively, see section 2.1(iii)). The segregation profiles of the $Pb_{95}Bi_5$(110) alloy surface calculated at different temperatures are presented in figure 6. As one can see, these segregation profiles are similar to those obtained for the $Pb_{95}Bi_5$(100) alloy surface, but a higher concentration of Bi in the surface layer is observed due to the higher positive value of the point interaction, $V^{(1)}_1 - V^{(1)}_{bulk}$, and one can also see a gradual decrease of Pb concentration on the second layer as the temperature increases. The point interactions, $V^{(1)}_\Lambda - V^{(1)}_{bulk}$, for $\Lambda = 2,3$, are also positive, but negligible compared to that quantity for $\Lambda = 1$, which determines the gradual decay of the segregation profiles between the second and third layers. However, one can see a weak oscillation of the segregation profiles between the fourth and sixth layers which can be also explained in terms of calculated ECI: $V^{(2)}_{\Lambda+} > V^{(2)}_\Lambda$ for $\Lambda = 1$–4.

Table 3. The CW effective cluster interactions for the $Pb_{95}Bi_5$(110) surface in K.

Λ	$V^{(1)}_\Lambda - V^{(1)}_{bulk}$	$V^{(2)}_\Lambda$	$V^{(2)}_{\Lambda+}$	$V^{(2)}_{\Lambda++}$	$V^{(3)}_{\Lambda+}$	$V^{(3)}_{\Lambda++}$	$V^{(3)}_{\Lambda+++}$	$V^{(4)}_\Lambda$
1	1054.70	83.04	650.19	−9.15	−41.41	−80.05	−2.38	76.15
2	34.23	134.28	354.58	119.24	−62.87	7.36	−31.33	−21.76
3	32.26	69.05	313.64	119.24	25.13	4.84	9.68	−21.76
4	0.00	74.42	313.64	119.24	4.84	4.84	9.68	−21.76

We conclude that strong oscillations of the segregation profiles for the $Pb_{95}Bi_5$(111) alloy surface are due to the coherency of this surface to the HCP (Mg-type) Pb_3Bi phase which is 'responsible' for these oscillations. Taking into account the possibility of a strong interaction between Ni and Bi, which is present at high concentrations relative to the bulk in both the first and third layers of the $Pb_{95}Bi_5$(111) alloy surface, we selected this surface for further investigation of co-segregation phenomena in the Pb–Bi–Ni system.

5. Results of *ab initio* calculation of the segregation profiles for the $Pb_{95}Bi_5Ni$(111) alloy surface

5.1. Segregation energy calculations

We have calculated the segregation energies for Bi and Ni to different layers of Pb(111) and $Pb_{95}Bi_5$(111) alloy surfaces by using (13). The segregation energies of Bi and Ni to the first layer of the Pb(111) surface are −0.104 eV/atom and 0.941 eV/atom, respectively. In contrast to Bi, Ni does not segregate to the first Pb(111) surface layer. Moreover, Ni does not segregate to the subsurface layers (the segregation energy is ∼0.2 eV for the second and the third layers and vanishes for deeper layers).

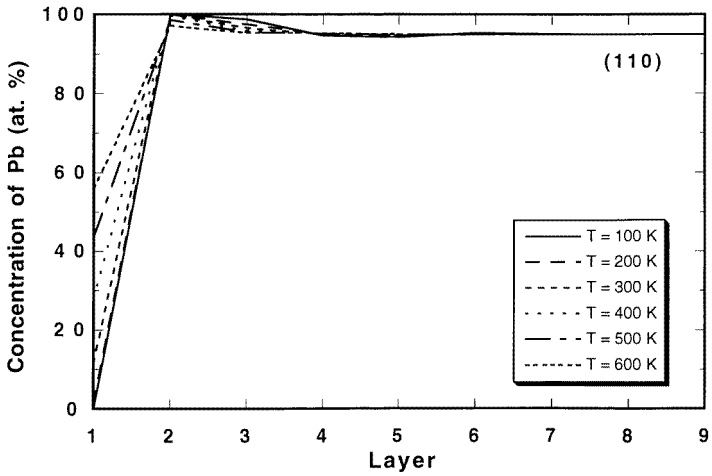

Figure 6. *Ab initio* calculated equilibrium segregation profiles at the (110) surface of the disordered $Pb_{95}Bi_5$ alloy at the indicated temperatures.

For the equilibrium $Pb_{95}Bi_5(111)$ alloy surfaces, we find a different kind of behaviour. As can be seen from table 4, where we summarize the segregation energies of Ni on the first and second surface layer calculated on the basis of the LMTO–CPA, Ni still does not segregate to the $Pb_{95}Bi_5(111)$ alloy first surface layer. However, its segregation energy drops significantly in comparison with the corresponding value for the Pb(111) surface. The segregation energy of Ni to the second layer is negative over the whole temperature interval under consideration: at $T = 100$ K, the energy of segregation of Ni to the second layer of the $Pb_{95}Bi_5(111)$ alloy is -0.103 eV/atom which is almost the same as the segregation energy of Bi to the first layer of Pb(111) (-0.104 eV/atom). For deeper $Pb_{95}Bi_5(111)$ alloy surface layers, the segregation energy of Ni is almost equal to zero. Thus, the segregation of Bi on the first and the third $Pb_{95}Bi_5(111)$ alloy surface layers promotes the segregation of Ni on the second layer, which is only occupied by Pb atoms at low temperatures. As the temperature increases to about 700 K, the absolute value of the segregation energy of Ni on the second layer decreases and reaches ~ 0.015 eV/atom ≈ 0 (within the accuracy of our method), reflecting the disappearance of Bi–Ni co-segregation.

Table 4. Segregation energies (in eV/atom) of Ni on the $Pb_{95}Bi_5(111)$ surface at different temperatures.

Λ	100 K	300 K	500 K	700 K
1	0.550	0.454	0.538	0.588
2	−0.103	−0.072	−0.030	−0.015

5.2. Calculation of the segregation profiles

In order to calculate the ECI for the Pb–Bi–Ni(111) alloy surface, we performed calculations of the concentration profiles given in table A1 for Pb_cBi_{1-c}, Pb_cNi_{1-c} and Bi_cNi_{1-c} alloys with bulk concentration $c = 0.5$. In each case, the individual atomic sphere radii were again set equal to the average atomic Wigner–Seitz radius (3.6557 au) of the bulk $Pb_{95}Bi_5$ alloy for

which all the surface calculations were performed. Unfortunately, the ASA approximation did not lead to convergence of the concentration profiles with predominant concentrations of Ni in adjoining layers (profiles No 6, 19, 24, 35 and No 6, 18, 19, 23, 24, 35 for Pb–Ni and Bi–Ni systems, respectively) presumably because it could not accommodate the large size mismatch between Ni and Pb (or Bi) atoms. The only values we obtained from these concentration profile calculations are the on-site interactions (i.e. the segregation energies of Pb and Bi species at $Pb_{50}Ni_{50}$ and $Bi_{50}Ni_{50}$(111) surfaces): $V_{\Lambda}^{(1)} - V_{bulk}^{(1)} = -1800.95$ K ($\Lambda = 1$), -555.46 K ($\Lambda = 2$), -17.81 K ($\Lambda = 3$) and -2834.66 K ($\Lambda = 1$), -6.59 K ($\Lambda = 2$), 138.78 K ($\Lambda = 3$) for Pb–Ni and Bi–Ni, respectively. To obtain the remaining surface ECI, we calculated the bulk ECI following the general scheme of Connolly and Williams [7], as expanded by Lu *et al* [46] for next-nearest neighbours. These bulk ECIs are presented in table 5. Here $V_n^{(2)}$ is the pair ECI in the nth coordination shell ($n = 1$–4) and $V_1^{(3)}$ and $V_1^{(4)}$ are three-site and four-site nearest-neighbour ECIs, respectively.

Table 5. The two-, three- and four-site effective cluster interactions (in K).

	Pb–Ni	Bi–Ni
$V_1^{(2)}$	2865.28	4191.90
$V_1^{(3)}$	−302.90	−307.60
$V_1^{(4)}$	76.63	23.38
$V_2^{(2)}$	−312.01	−712.47
$V_3^{(2)}$	−321.53	−545.83
$V_4^{(2)}$	0.00	0.00

The nearest and next-nearest ECIs for the Pb–Bi–Ni alloy (111) surface are presented in table 6. Figures 7(a) and 7(b) show the calculated equilibrium segregation profiles for Bi and Ni, respectively on the (111) surface of a random $Pb_{95}Bi_5 + 0.05$ at.% Ni alloy at several different temperatures. As one can see, Ni does not co-segregate with Bi to the Pb(111) surface. These results are obtained in the single-site mean-field approximation, i.e. without taking into account any possibility for ordering effects in the Pb–Bi–Ni system, and to some extent they are consistent with high-temperature experimental data: there is no Ni in the first two surface layers. On the other hand, one can find out that the ECI between Bi and Ni ($V_{\Lambda}^{(2)BiNi}$, $V_{\Lambda+}^{(2)BiNi}$) are large and positive, especially the intralayer interaction. Thus, there should be a strong ordering tendency in the layers. The Bi–Ni phase diagram [38, 47] shows the existence of two compounds: the β-phase (BiNi) which has a NiAs type hexagonal structure, and Bi_3Ni which has a rhombic lattice. One cannot exclude the possibility that the ternary system consists of a mixture of at least two phases: a Pb–Bi random phase and one of the ordered binary Bi–Ni phases, or maybe a ternary Bi–Ni–Pb phase. To study these phenomena, we performed MC simulation of surface segregation in Pb–Bi, Pb–Ni and Pb–Bi–Ni systems, including both relaxation and vibration effects. Before presenting these results in section 6, we address the formation of ordered structures on the subsurface layers of Pb–Bi–Ni alloys within the framework of the *ab initio* formalism.

5.3. Ordered structures on the subsurface layers of Pb–Bi–Ni alloys

As mentioned above, there is a tendency of Ni to segregate to the second layer of the $Pb_{95}Bi_5$ alloy (111) surface at low temperatures. In order to estimate the range of Ni segregation to this layer, we calculated the surface energy of the $Pb_{95}Bi_5$(111) alloy with equilibrium

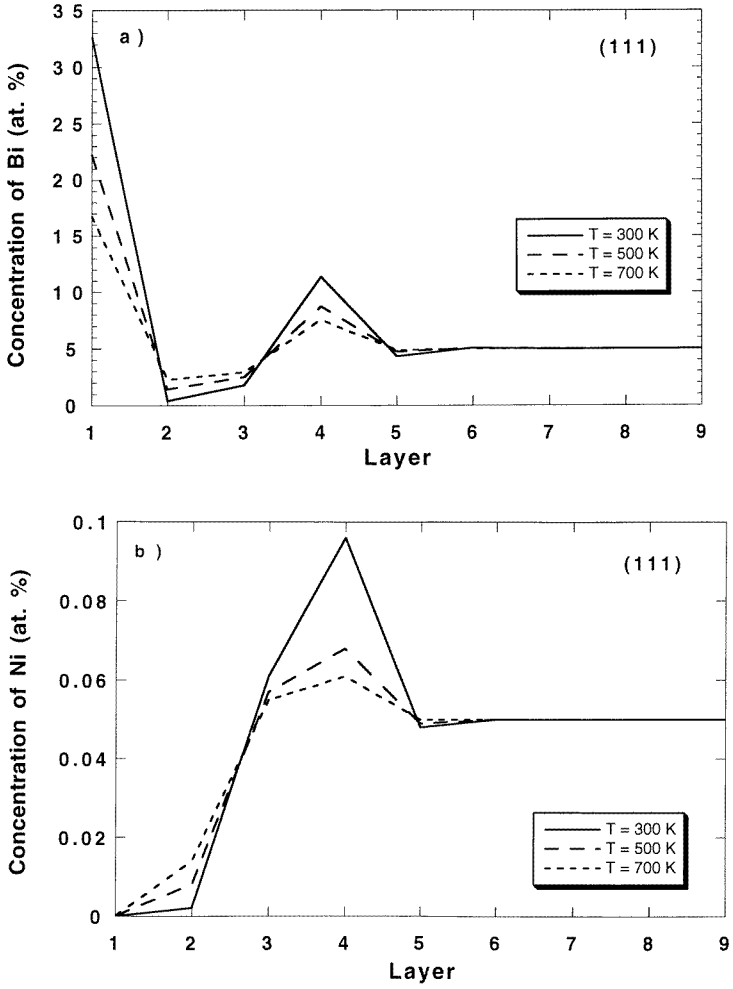

Figure 7. *Ab initio* calculated equilibrium segregation profiles of (a) Bi and (b) Ni at the (111) surface of the disordered $Pb_{95}Bi_5 + 0.05$ at.% Ni alloy at the indicated temperatures.

segregation profile at $T = 100$ K (see figure 4):

$$Pb_{4.3}Bi_{95.7}/Pb/Pb_{73.7}Bi_{26.3}/Pb_{97.6}Bi_{2.4}/Pb_{87.9}Bi_{12.1}/4Pb_{95}Bi_5. \tag{14}$$

By substituting some fraction of the Pb atoms in the second layer with Ni atoms, and comparing the surface energy of the new slab with that of the original one, we found that exceeding a concentration of 12 at.% Ni in the second layer is energetically unfavourable. Christensen *et al* [45] have pointed out that low-solubility elements, which do not segregate to the surface layer because their surface energies are too high, may show a tendency to segregate to the (second) subsurface layer. In addition, in miscible systems, with a tendency to form a bulk ordered phase, a high-surface-energy solute may form subsurface ordered phases. These considerations apply to binary systems. In the present ternary system, the situation will clearly be more complex, but the above results illustrate the possibility that Pb–Bi–Ni alloys will show the formation of subsurface ordered Bi–Ni layers.

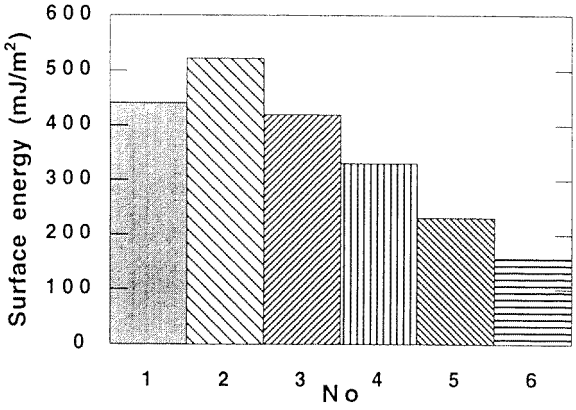

Figure 8. Calculated surface energies for different configurations forming on the $Pb_{95}Bi_5$ + Ni(111) surface.

Table 6. The CW and CF effective cluster interactions for the Pb–Bi–Ni(111) surface in K.

	CW							
Λ	$V^{(1)}_{\Lambda;PbBi}$	$V^{(1)}_{\Lambda;PbNi}$	$V^{(2)}_{\Lambda;PbBi}$	$V^{(2)}_{\Lambda+PbBi}$	$V^{(2)}_{\Lambda;PbNi}$	$V^{(2)}_{\Lambda+PbNi}$	$V^{(2)}_{\Lambda;BiNi}$	$V^{(2)}_{\Lambda+BiNi}$
1	−499.38	1800.95	231.54	370.45	1352.3	960.0	1959.6	1110.5
2	505.32	555.46	190.13	203.77	1352.3	960.0	1959.6	1110.5
3	327.27	17.81	192.33	307.65	1352.3	960.0	1959.6	1110.5
4	0.00	0.00	191.36	191.36	1352.3	960.0	1959.6	1110.5

	CF		
Λ	$V^{(2)}_{\Lambda++;PbBi}$	$V^{(2)}_{\Lambda++;PbNi}$	$V^{(2)}_{\Lambda++;BiNi}$
1–4	−133.05	−80.38	−136.46

As one can see from expression (14), there is a predominant amount of Bi in the surface layer, and the amount of Bi in the third subsurface layer also exceeds the bulk concentration of Bi in the alloy by more than 10%. As mentioned above, the Bi–Ni bulk phase diagram [38, 47] shows that there is only one ordered phase in the Bi-rich region, Bi_3Ni, which has a rhombic structure. However, the probability of formation of this structure at the FCC (111) surface is small. For example, experiments have shown that the symmetry of epitaxially grown layers, such as HCP metals on FCC metals, is usually FCC up to four or five layers. If one expected ordering to occur in the first two or three subsurface layers, the ordered structure at the (111) surface of Pb–Bi–Ni would most likely display FCC symmetry. That is why we selected a hypothetical Bi_3Ni compound having the $L1_2$ structure as the prototype phase forming on the surface under consideration.

In figure 8 we summarize the calculated surface energies for different configurations forming on the $Pb_{95}Bi_5$ + Ni(111) surface. As one can see, configuration No 2 (Pb in the second layer is substituted by a disordered $Bi_{75}Ni_{25}$ alloy) is unfavourable in comparison with the original configuration No 1. However if the $Bi_{75}Ni_{25}$ alloy orders to form a Bi_3Ni ($L1_2$) compound in the second subsurface layer (configuration No 3), then the surface

energy drops below the surface energy of the configuration No 1. This effect becomes even more significant, if the ordered Bi_3Ni ($L1_2$) phase forms on the third, fourth and fifth subsurface layers (configurations No 4–6). Of course, since the formation of the ordered phase should influence the composition of the surface layer, the problem should be solved self-consistently. However, this simple example shows how an ordered phase could form in the subsurface layers, covered by a surface layer of substrate material.

6. MC simulation of the segregation profiles on Pb–Bi, Pb–Ni and Pb–Bi–Ni(111) alloy surfaces

6.1. $Pb_{95}Bi_5$(111) alloy surface

Figure 9(a) shows the calculated equilibrium concentration profiles for the (111) surface of a $Pb_{95}Bi_5$ alloy at 300 K, 400 K and 500 K. The durations of the MC runs were 300 000 MCS/A, 500 000 MCS/A and 750 000 MCS/A for 500 K, 400 K and 300 K, respectively. The profiles obtained are oscillatory, with a strong segregation of Bi to the first surface layer and a slight depletion of Bi in the second layer. These results are in fair agreement with results of the *ab initio* calculations of the segregation profiles discussed in section 4.1 and shown in figure 9(b).

6.2. PbNi(111) alloy surface

The MC equilibration of the 'surface' computational cell at $T = 500$ K ($a = 4.9722$ Å, 200 000 MCS/A) did not show any evidence of Ni segregation to the outermost Pb(111) surface layer. This is in accord with the results of our *ab initio* calculations (see section 5.1). However, the present calculations show a segregation of Ni to the second layer ($\sim$0.14 at.%) which was not detected by the *ab initio* method. This difference could be due to strain energy effects, which are not accounted for in the 'unrelaxed' *ab initio* calculations but which could arise from atomic relaxation in the MC simulations. Recent experimental observations in binary Pb–Ni alloys [48] show no measurable Ni segregation to the surface up to the solubility limit of Ni in Pb. Thus, the present results are also consistent with these experiments, as the predicted segregation of Ni to the second surface layer is too small to be detected experimentally.

6.3. PbBiNi(111) alloy surface

Figures 10(a) and 10(b) show the calculated equilibrium concentration profiles of Bi and Ni for the (111) surface of a $Pb_{95}Bi_5 + 0.05$ at.% Ni alloy at 500 K. In order to reach equilibrium, we performed the MC run with duration of 2 500 000 MCS/A. On the surface layer, a low concentration of Ni ($\sim$4 at.%) is observed, and the concentration of Bi increases from 7.5 at.% for the binary $Pb_{95}Bi_5$ alloy to $\sim$26 at.% in the ternary alloy. On the second layer, the concentrations of Bi and Ni are almost equal ($\sim$20 at.%). On the third layer, the concentration of Bi reaches $\sim$26 at.% again, and concentration of Ni drops to a level of 7 at.%. The concentration of Ni decreases gradually as distance from the surface increases and approaches the bulk composition at the seventh layer. In the case of the ternary Pb–Bi–Ni alloy, oscillations of the Bi segregation profile are more pronounced. Results of the MC simulation also clearly show a strong tendency for Bi and Ni to co-segregate to the surface.

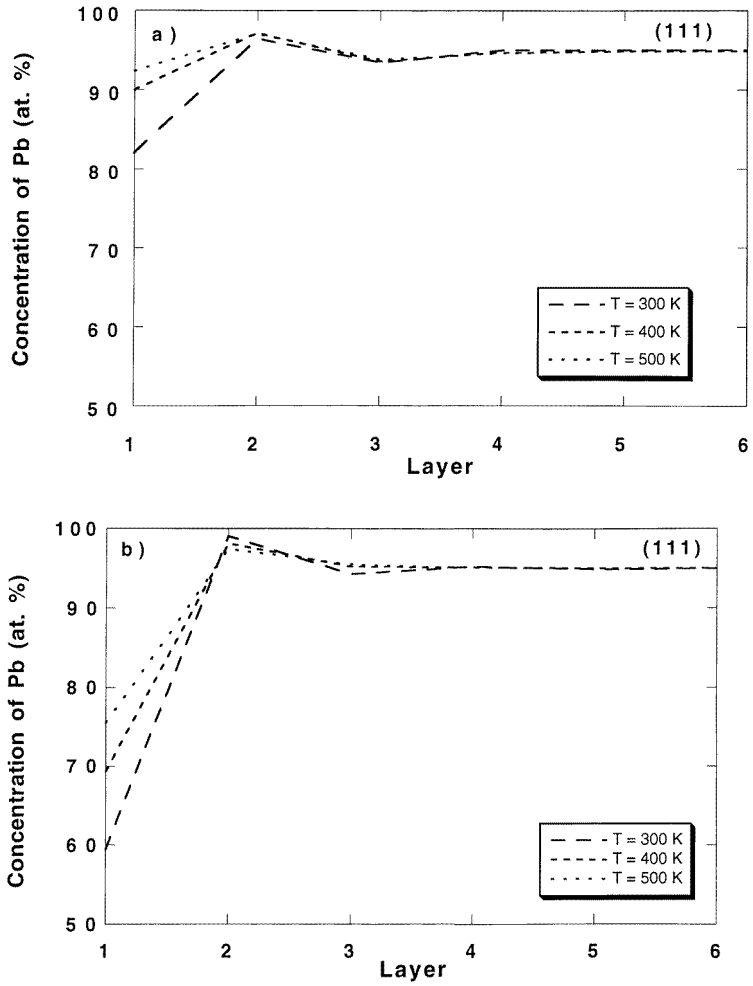

Figure 9. Calculated equilibrium segregation profiles at the (111) surface of the $Pb_{95}Bi_5$ alloy at the indicated temperatures. (a) MC (FS potential); (b) *ab initio* (LMTO).

7. Conclusions

In the present manuscript we have demonstrated that segregation profiles at the surface of a $Pb_{95}Bi_5$ alloy depend on the particular surface orientation. We conclude that strong oscillations of the segregation profiles for the $Pb_{95}Bi_5(111)$ alloy surface are due to the coherency of this surface with the HCP (Mg-type) Pb_3Bi phase which induces these oscillations. While Ni does not segregate to the Pb(111) surface, it shows a tendency to segregate to the subsurface layer of the $Pb_{95}Bi_5(111)$ alloy, due to its strong interaction with Bi, which is present at high concentrations relative to the bulk in both the first and third atom layers of the $Pb_{95}Bi_5(111)$ alloy surface. While the *ab initio* approach allows one to obtain a rough picture of surface phenomena in $Pb_{95}Bi_5$ and $Pb_{95}Bi_5 + Ni$ alloys, consideration of vibration and relaxation effects, e.g. within the MC formalism, are clearly essential to any detailed comparison with experimental results. By segregating to the subsurface (second) layer, Ni 'promotes' additional segregation of Bi to the first three surface layers, which,

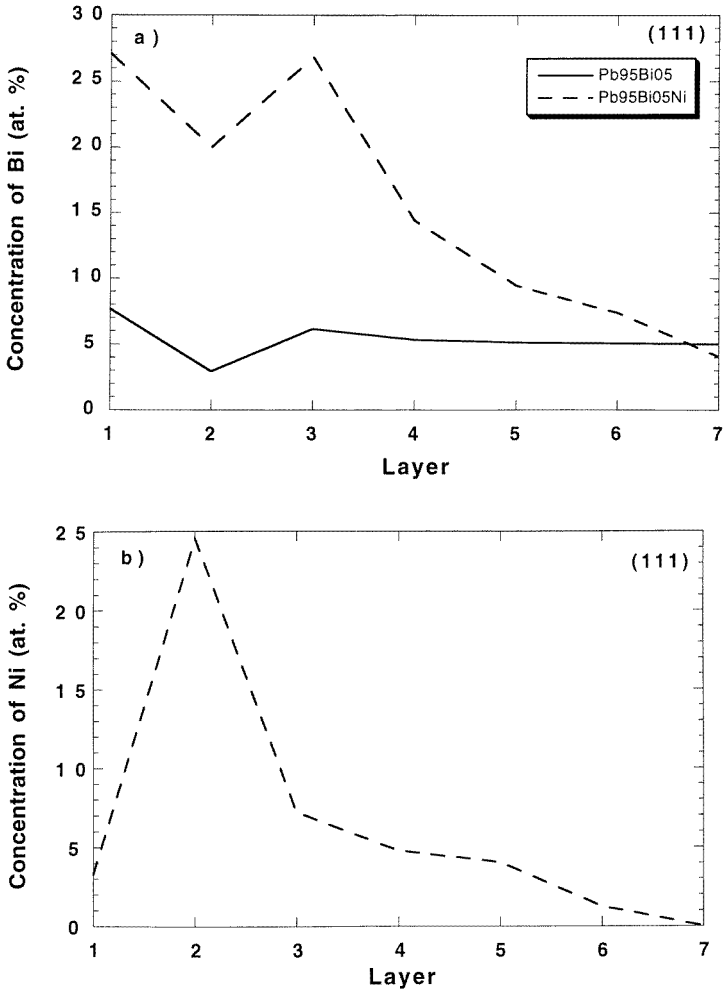

Figure 10. Calculated (MC) equilibrium segregation profiles of (a) Bi and (b) Ni at the (111) surface of the $Pb_{95}Bi_5$ (a) and $Pb_{95}Bi_5 + 0.05$ at.% Ni ((a) and (b)) alloys at $T = 500$ K.

in turn, drives further segregation of Ni to the surface layer. We expect that these co-segregation phenomena will be more pronounced at low temperatures: MC calculations for $T = 400$ K are currently under way.

Acknowledgments

Support by the National Science Foundation is gratefully acknowledged by PW and AL under grant DMR9530469, and by AG and VV under grant DMR9626344. AR and HS wish to acknowledge support by the Danish National Research Foundation. The authors also wish to thank Drs S Foiles and M Yan for providing the Monte Carlo codes used in this study, and Drs A Lichtenstein and O Mryasov for performing the full-potential LMTO calculations. Last but not least, we acknowledge with thanks the Pittsburgh Supercomputing Center for access to their supercomputing facilities under grant DMR930031P.

Appendix

Table A1. The configurations used in the self-consistent LMTO–CPA calculations in order to determine ECIs for $A_cB_{1-c}(111)$ alloy surface ($d = 0.75$; $e = 0.2$). The concentrations within the fifth and within all other layers were equal to the concentration of the bulk.

Λ	1	2	3	4	5	6	7	8	9	10	11	12	13	14	15	16	17	18	19	20
1	*c*	A	B	A	B	B	A	*c*	*c*	*c*	*c*	*c*	*c*	*d*	*c*	*c*	*c*	B	*c*	*c*
2	*c*	*c*	*c*	B	A	B	A	A	B	*c*	*c*	*c*	*c*	*c*	*d*	*c*	*c*	*e*	B	A
3	*c*	*c*	*c*	*c*	*c*	*c*	*c*	*c*	*c*	B	A	*c*	*c*	*c*	*c*	*d*	*c*	*c*	B	A
4	*c*	*c*	*c*	*c*	*c*	*c*	*c*	*c*	*c*	*c*	*c*	B	A	*c*	*c*	*c*	*d*	*c*	*c*	*c*

Λ	21	22	23	24	25	26	27	28	29	30	31	32	33	34	35	36	37	38	39
1	*c*	*c*	*c*	*c*	*c*	*c*	*c*	*c*	*e*	*c*	*c*	A	A	B	B	*c*	*c*	*c*	*c*
2	B	A	*e*	*c*	*c*	*c*	*c*	*c*	*d*	*d*	*c*	*c*	*c*	*c*	*c*	A	A	B	B
3	A	B	B	B	A	B	A	*e*	*c*	*e*	*d*	A	B	A	B	*c*	*c*	*c*	*c*
4	*c*	*c*	*c*	B	A	A	B	B	*c*	*c*	*e*	*c*	*c*	*c*	*c*	A	B	A	B

Table A2. The configurations used in the self-consistent LMTO–CPA calculations in order to determine ECI for the $A_cB_{1-c}(100)$ alloy surface. The concentrations within the fifth and within all other layers were equal to the concentration of the bulk.

Λ	1	2	3	4	5	6	7	8	9	10	11	12	13	14	15
1	*c*	A	B	B	A	A	B	*c*	*c*	*c*	*c*	*c*	*c*	*c*	*c*
2	*c*	*c*	*c*	A	B	A	B	A	*c*	*c*	*c*	A	B	B	*c*
3	*c*	*c*	*c*	*c*	*c*	*c*	*c*	*c*	A	*c*	*c*	A	B	A	A
4	*c*	*c*	*c*	*c*	*c*	*c*	*c*	*c*	*c*	A	B	*c*	*c*	*c*	B

Λ	16	17	18	19	20	21	22	23	24	25	26	27	28	29
1	*c*	*c*	*c*	*c*	*c*	*c*	A	A	B	B	*c*	*c*	*c*	*c*
2	*c*	B	*c*	A	*c*	*c*	*c*	*c*	*c*	*c*	A	A	B	B
3	B	*c*	B	B	B	A	A	B	A	B	*c*	*c*	*c*	*c*
4	A	*c*	*c*	*c*	B	A	*c*	*c*	*c*	*c*	A	B	A	B

Table A3. The configurations used in the self-consistent LMTO–CPA calculations in order to determine ECIs for $A_cB_{1-c}(110)$ alloy surface. The concentrations within the fifth and within all other layers were equal to the concentration of the bulk.

Λ	1	2	3	4	5	6	7	8	9	10	11	12	13	14	15
1	*c*	A	B	*c*	*c*	*c*	*c*	*c*	*c*	A	B	A	*c*	*c*	*c*
2	*c*	*c*	*c*	A	B	*c*	*c*	*c*	*c*	A	A	B	A	B	A
3	*c*	*c*	*c*	*c*	*c*	A	B	*c*	*c*	*c*	*c*	*c*	A	A	B
4	*c*	*c*	*c*	*c*	*c*	*c*	*c*	A	B	*c*	*c*	*c*	*c*	*c*	*c*

Λ	16	17	18	19	20	21	22	23	24	25	26	27
1	*c*	*c*	*c*	A	B	B	*c*	*c*	*c*	B	*c*	*c*
2	*c*	*c*	*c*	*c*	B	A	A	B	B	B	B	*c*
3	A	B	A	B	A	A	*c*	B	A	*c*	B	B
4	A	A	B	*c*	*c*	*c*	B	A	A	*c*	*c*	B

References

[1] Cheng W-C and Wynblatt P 1997 *J. Cryst. Growth* **173** 513
[2] Cheng W-C and Wynblatt P 1996 *Surf. Sci.* **364** 409
[3] Carlsson A E 1990 *Solid State Physics* vol 43 (New York: Academic) p 1
[4] Skriver H L and Rosengaard N M 1991 *Phys. Rev.* B **43** 9538
[5] Abrikosov I A and Skriver H L 1993 *Phys. Rev.* B **47** 16 532
[6] Monnier R 1997 *Phil. Mag.* B **75** 67
[7] Connolly J W D and Williams A R 1983 *Phys. Rev.* B **27** 5169
[8] Gunnarsson O, Jepsen O and Andersen O K 1983 *Phys. Rev.* B **27** 7144
[9] Andersen O K and Jepsen O 1984 *Phys. Rev. Lett.* **53** 2571
[10] Andersen O K, Jepsen O and Glötzel D 1985 *Highlights of Condensed-Matter Theory* ed F Bassani, F Fumi and M P Tosi (New York: North-Holland) p 59
[11] Andersen O K, Pawlowska Z and Jepsen O 1986 *Phys. Rev.* B **34** 5253
[12] Lambrecht W R L and Andersen O K 1986 *Surf. Sci.* **178** 256
[13] Ruban A V, Abrikosov I A, Kats D Y, Gorelikov D, Jacobsen K W and Skriver H L 1994 *Phys. Rev.* B **49** 11 383
[14] Abrikosov I A, Ruban A V, Skriver H L and Johansson B 1994 *Phys. Rev.* B **50** 2039
[15] Ruban A V and Skriver H L 1997 *Phys. Rev.* B **55** 8801
[16] Christensen A, Ruban A V and Skriver H L 1997 *Surf. Sci.* **383** 235
[17] Hansen P L, Molenbroek A M and Ruban A V 1997 *J. Phys. Chem.* **101** 1861
[18] Landa A, Wynblatt P, Girshick A, Vitek V, Ruban A and Skriver H 1998 *Acta Mater.* **46** 3027
[19] Sanchez J M and de Fontaine D 1981 *Structure and Bonding in Crystals* ed M O'Keefe and A Navrotsky (New York: Academic) p 117
[20] Vaks V G, Zenin N E and Kamyshenko V V 1988 *J. Phys. F: Met. Phys.* **18** 1641
Vaks V G, Zenin N E and Kamyshenko V V 1989 *J. Phys.: Condens. Matter* **1** 2115
[21] Steinberg A S, Kats D Ya and Men B A 1992 *Phys. Status Solidi* B **174** 9
[22] Sanchez J M, Ducastelle F and Gratias D 1984 *Physica* A **128** 334
[23] Foiles S M 1985 *Phys. Rev.* B **32** 7685
[24] Hoffmann M A and Wynblatt P 1990 *Surf. Sci.* **236** 369
[25] Liu Y and Wynblatt P 1990 *Surf. Sci.* **240** 245
[26] Daw M S and Baskes M I 1984 *Phys. Rev.* B **29** 6443
[27] Ercolessi F, Parinello M and Tosatti E 1988 *Phil Mag.* A **58** 213
[28] Lim H S, Ong C K and Ercolessi F 1992 *Surf. Sci.* **269/270** 1109
[29] Finnis M W and Sinclair J E 1984 *Phil. Mag.* A **50** 45
Finnis M W and Sinclair J E 1986 *Phil. Mag.* A **53** 161
[30] Ackland G J, Tichy G, Vitek V and Finnis M W 1987 *Phil. Mag.* A **56** 735
[31] Ackland G J and Vitek V 1990 *Phys. Rev.* B **41** 10 324
[32] Vitek V, Ackland G J and Cserti J 1991 *Mater. Res. Soc. Symp. Proc.* vol 186, ed G M Stocks, D P Pope and A F Giamei (Pittsburgh, PA: Materials Research Society) p 237
[33] Yan M, Šob M, Luzzi D E, Vitek V, Ackland G J, Methfessel M and Rodriguez C O 1993 *Phys. Rev.* B **47** 5571
[34] Methfessel M 1988 *Phys. Rev.* B **38** 1537
[35] Ruban A V, Abrikosov I A and Skriver H L 1995 *Phys. Rev.* B **51** 12 958
[36] Perdew J and Zunger A 1981 *Phys. Rev.* B **23** 5048
[37] Ceperley D M and Alder B J 1980 *Phys. Rev. Lett.* **45** 566
[38] Vol A E 1966 *Handbook of Binary Metallic Systems: Structure and Properties* (Jerusalem: Israel Program for Scientific Translations)
[39] Gunningham S L 1974 *Phys. Rev.* B **10** 4988
[40] Moruzzi V L, Janak J F and Schwartz K 1988 *Phys. Rev.* B **37** 790
[41] Heyraud J C and Metois J J 1983 *Surf. Sci.* **128** 334
[42] Landa A, Wynblatt P, Häkkinen H, Barnett R N and Landman U 1995 *Phys. Rev.* B **51** 10 972
[43] Landa A and Wynblatt P 1997 *Comput. Mater. Sci.* **7** 257
[44] Landa A I, Ruban A V, Abrikosov I A, Wynblatt P and Skriver H L 1997 *Mater. Res. Soc. Symp. Proc.* vol 440, ed R C Cammarata, E H Chason, T L Einstein and E D Williams (Pittsburgh, PA: Materials Research Society) p 467
[45] Christensen A, Ruban A V, Stoltze P, Jacobsen K W, Skriver H L, Nørskov J K and Besenbacher F 1997 *Phys. Rev.* B **56** 5822
[46] Lu Z W, Wei S-H, Zunger A, Frota-Pessoa S and Ferreira L G 1991 *Phys. Rev.* B **44** 5121
[47] Hansen M and Anderko K 1958 *Constitution of Binary Alloys* (New York: McGraw-Hill)
[48] Wang Z and Wynblatt P 1997 private communication